Validating a Monotonically-Integrated Large Eddy Simulation Code for Subsonic Jet Acoustics

Daniel Ingraham* and James Bridges†

National Aeronautics and Space Administration, John H. Glenn Research Center, Cleveland, OH, 44135, USA

The results of subsonic jet validation cases for the Naval Research Lab's Jet Engine Noise REduction (JENRE) code are reported. Two set points from the Tanna matrix, set point 3 ($M_a = 0.5$, unheated) and set point 7 ($M_a = 0.9$, unheated) are attempted on three different meshes. After a brief discussion of the JENRE code and the meshes constructed for this work, the turbulent statistics for the axial velocity are presented and compared to experimental data, with favorable results. Preliminary simulations for set point 23 ($M_a = 0.5$, $T_j/T_\infty = 1.764$) on one of the meshes are also described. Finally, the proposed configuration for the farfield noise prediction with JENRE's Ffowcs-Williams Hawking solver are detailed.

Nomenclature

x, y, z	Cartesian coordinates, with origin at the nozzle exit and centerline, x indicating the axial coordinate, increasing downstream
r	Radial coordinate, $r^2 = y^2 + z^2$
Δ	Approximate mesh spacing
L	Length of the mesh region meant to resolve the turbulent nearfield
D_j	Exit diameter of the nozzle
U_j	Fully-expanded jet exit velocity
$\overline{U}$, U'	Mean and root-mean square of axial velocity, respectively
T_j	Fully-expanded jet exit temperature
$\overline{T}$, T'	Mean and root-mean square of temperature, respectively
T_0, T	Startup and statistics-gathering simulation times, respectively
θ	Polar angle, with $\theta = 0$ pointing upstream (i.e. the negative-x direction)
y_τ	Estimate of viscous length scale in the nozzle boundary layer

I. Introduction

Considerable effort has been invested by the computational aeroacoustic community in the prediction of subsonic jet noise through large eddy simulation (LES)[1–20] (see also the excellent review from Bodony[21]). Most of this work has been focused on using codes that employ high-order finite difference or finite volume schemes and structured grids in their discretization of the governing equations. A number examples of the application of *unstructured* LES codes to the problem of supersonic jet noise can also be found in the literature, e.g., the work done by researchers associated with Cascade Technologies[22–26] and the Naval Research Laboratory (NRL).[27–33] Comparably little work has been done to validate the effectiveness of unstructured LES codes at simulating the acoustics of subsonic jets. While not needed to capture the geometry of the simple nozzles considered in this paper, the flexibility provided by unstructured meshes allows users to use small cell sizes in localized areas of the flow without affecting the mesh downstream, unlike structured meshes. Also, simulating the subsonic regime of jet flows approximating the takeoff condition is of interest to NASA's Commercial Supersonic Technology (CST) project, with the goal of providing acoustic predictions through traditional Ffowcs-Williams Hawking techniques[34] and more sophisticated methods (e.g.,

*Acoustics Branch, MS 54-3, AIAA Member

†Acoustics Branch, MS 54-3, AIAA Associate Fellow

the forthcoming Generalized Acoustic Analogy work of Leib et al.[35]). The combination of these needs has motivated addressing this gap in the literature.

The Jet Engine Noise REduction (JENRE) application,[36] developed by the NRL, is a computational aeroacoustics code designed to provide farfield acoustic predictions of jets using the LES approach to the simulation of turbulent flow. JENRE follows the Monotonically Integrated LES (MILES)[37] philosophy of sub-grid scale modeling, relying on the inherent numerical dissipation of the code's schemes to capture the effect of the unresolved turbulent scales will have on the resolved unsteady flow. Numerical dissipation is provided by blending low- and high-order finite element schemes through the Flux-Corrected Transport (FCT) approach. Proponents of this approach claim that the numerical dissipation effectively acts as an implicit model for the turbulent sub-grid scales, citing as evidence modified equation analysis[38] and the results of applying such schemes to practical turbulent flows.[39,40] Numerous finite element schemes are available in the version of the JENRE code used in this work – here, the second-order Taylor-Galerkin scheme[41,42] has been chosen for spatial and temporal discretization, coupled with a lumped-mass Galerkin scheme through the (FCT) method.[43]

II. Test Case Parameters

The flow parameters for the simulations described in this work are taken from the Tanna matrix,[44] and are shown in Table 1. The nozzle geometry chosen for this work was SMC000, the baseline round nozzle from the Small Metal Chevron series developed at the NASA Glenn Research Center (GRC). Described in more detail by Bridges and Wernet,[46] SMC000 is an axisymmetric nozzle with a nominal two-inch exit diameter that has been subjected to extensive experimental investigation at the GRC.[45,46]

	Set Point 3	Set Point 7	Set Point 23
M	0.513	0.985	0.376
$M_a = U_j/a_\infty$	0.500	0.900	0.500
T_j/T_∞	0.950	0.835	1.764
p_0/p_j	1.197	1.860	1.102
$Re_j = \frac{\rho_j U_j D}{\mu_j}$	$5.99 \cdot 10^5$	$1.36 \cdot 10^6$	$2.06 \cdot 10^5$

Table 1. Set points used in this work.

Two mesh generation programs were used to create the meshes used in this work: Pointwise[47] and Gmsh.[48] The first two meshes, referred to here as PW0 and PW1, were created with the Pointwise program, while the third mesh, GM0, was created with Gmsh. All meshes used the same SMC000 nozzle geometry. The boundaries of the nearfield, sponge zone, and outer domain were also identical. Figure 1 shows a diagram of the relative locations of the nozzle geometry, nearfield mesh region, and sponge zone and outer mesh boundaries. Diagrams of PW0, PW1, and GM0's mesh spacing distributions are shown in Figures 2, 3, and 4, respectively. Comparison of 2 and 3 shows that PW0 and PW1 differ in the element sizes in the region just downstream of the nozzle exit to about $12.5D_j$, with PW0's spacing in the former axial location being twice as large as PW1's, and increasing to the $0.04D_j$ value more quickly. Figure 5 shows a crinkle slice of PW0's $z = 0$ surface, where the surface of the slice has been constructed from the mesh element surfaces intersected by the $z = 0$ plane. Enlargements centered on the nearfield region for for this same crinkle slice are shown for the PW0 and PW1 meshes, respectively, in Figures 9 and 10. The element edges are colored in blue in these two figures to make the differences in mesh density more apparent.

Inspection of Figure 4 shows the GM0 mesh used approximately the same mesh spacing sizes as the PW1 mesh; however, the mesh spacing grows more gradually from the minimum $0.005D_j$ to the maximum $0.04D_j$ value. GM0 also includes a refined region around the nearfield with target mesh spacing of about $0.05D_j$, intended to propagate acoustic disturbances to a Ffowcs-Williams Hawking integration surface. The impact of this change can be seen by comparing Figure 6 to Figure 11.

The PW0 and PW1 meshes contained approximately $15 \cdot 10^6$ and $27 \cdot 10^6$ nodes, respectively, while GM0, with its FW-H refinement region, has about $55 \cdot 10^6$. The nearfield region consists of a conical frustum of length $L = 25D_j$ with a diameter of D_j at the nozzle exit and diverging at a rate of 4°. The shape of the nearfield was chosen to capture the development of the jet's shear layer, and was informed by the shear layer

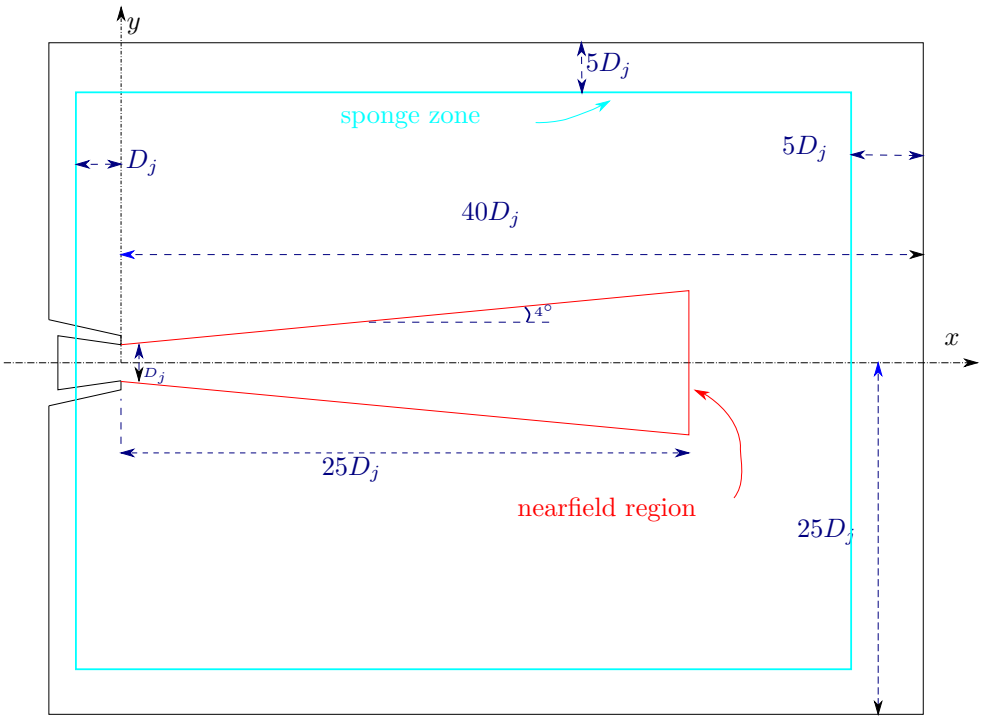

Figure 1. Diagram of the extent of the domain boundaries, including the size of the nearfield region and sponge zone.

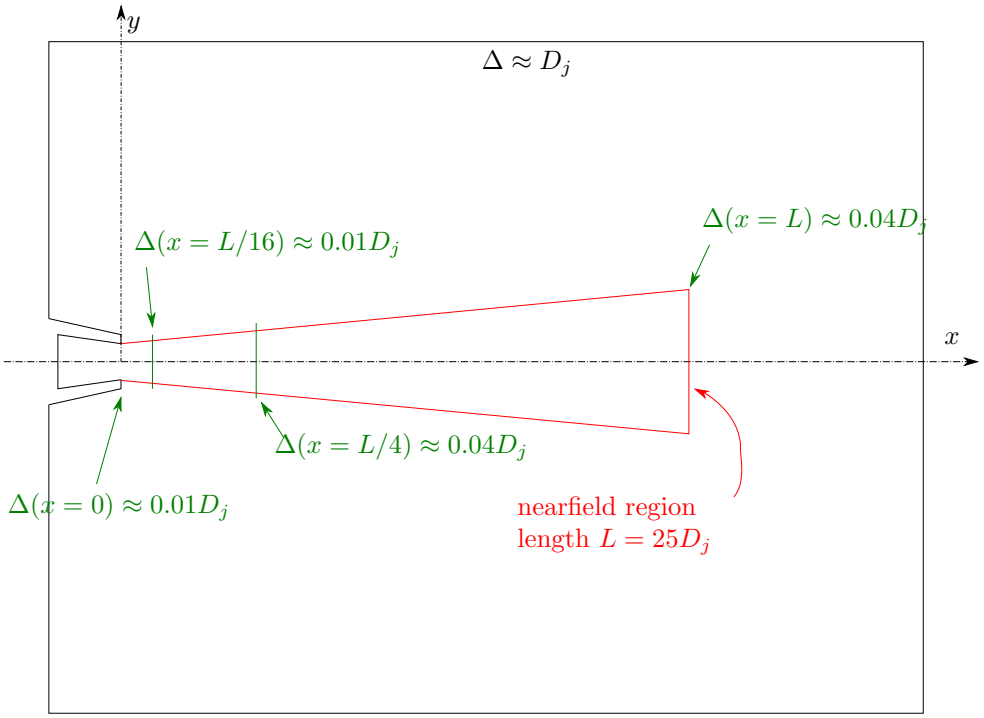

Figure 2. Approximate mesh spacing distribution for the PW0 mesh.

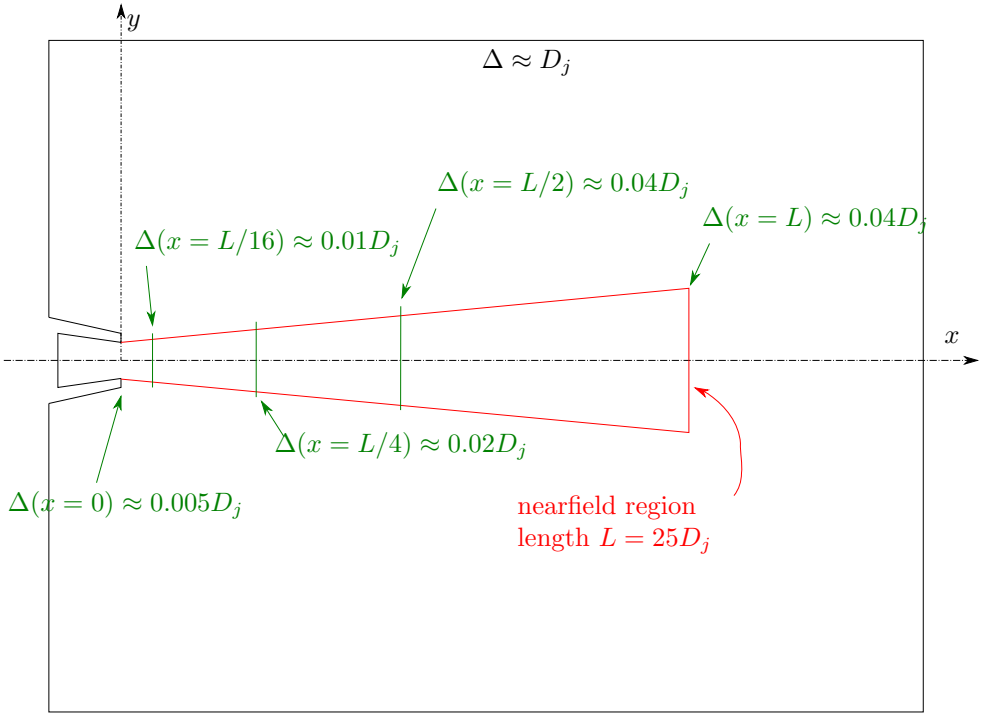

Figure 3. Approximate mesh spacing distribution for the PW1 mesh.

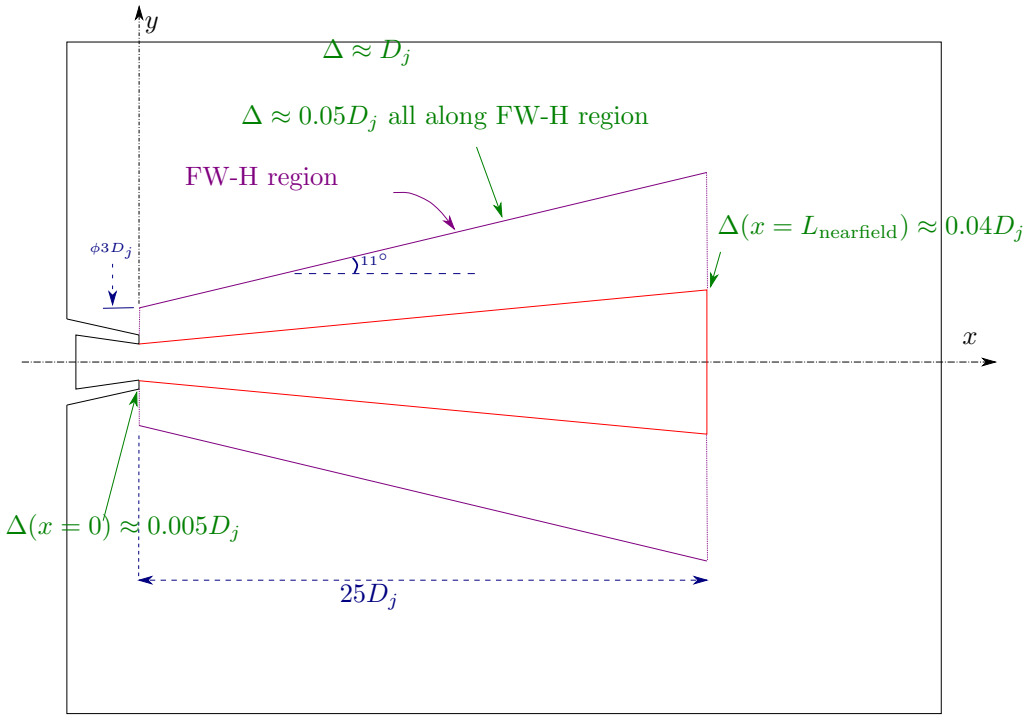

Figure 4. Approximate mesh spacing distribution for the GM0 mesh.

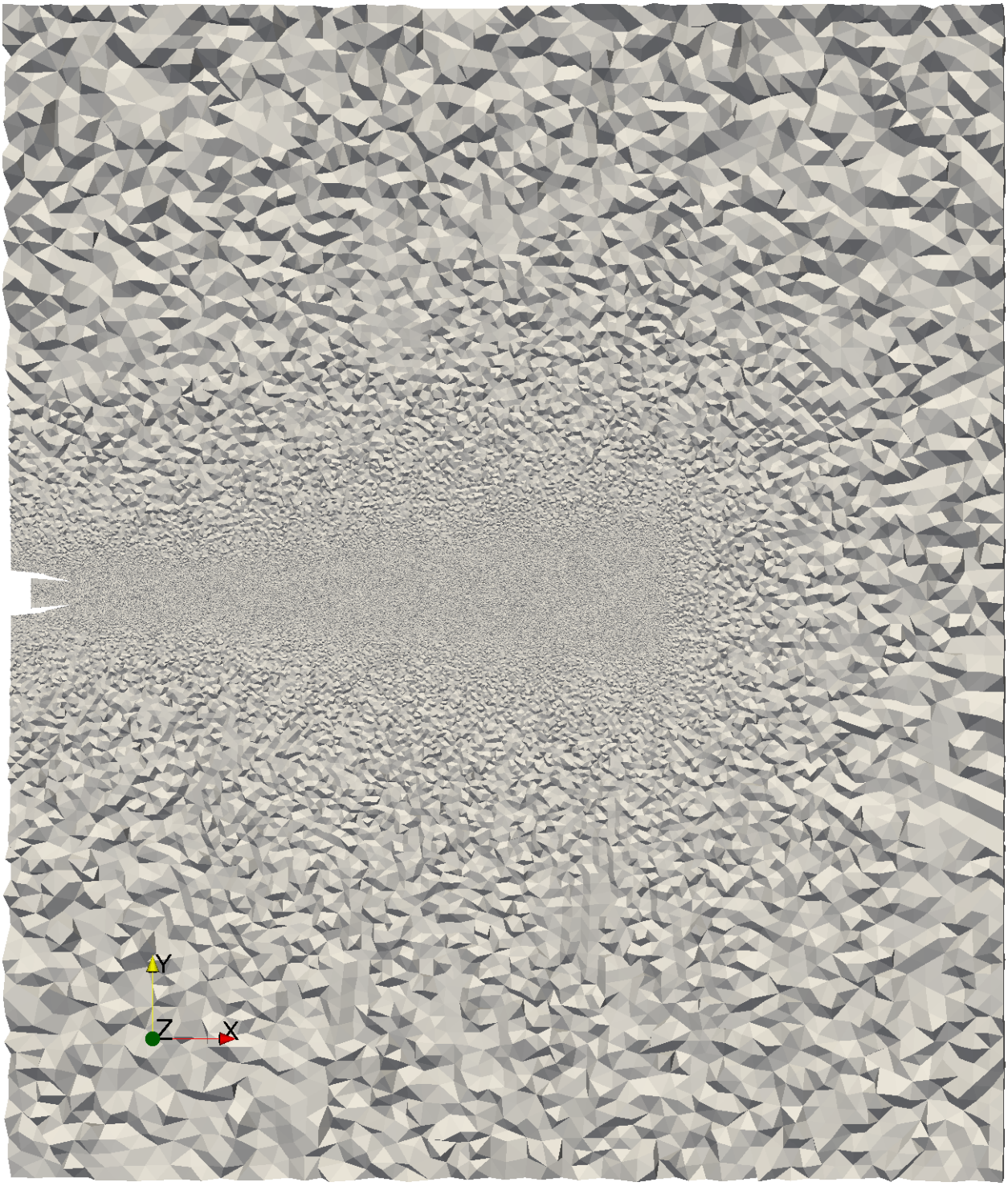

Figure 5. $z = 0$ **slice of the PW0 mesh.**

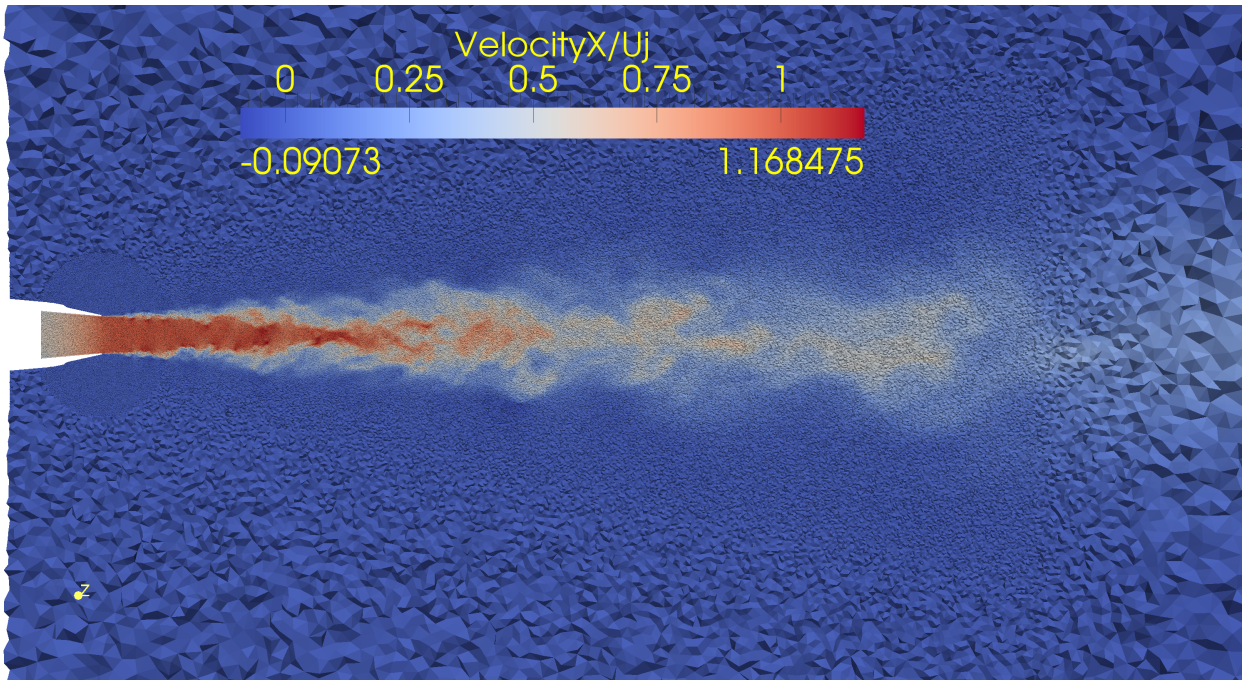

Figure 6. $z = 0$ **slice of the GM0 mesh, colored by instantaneous axial velocity.**

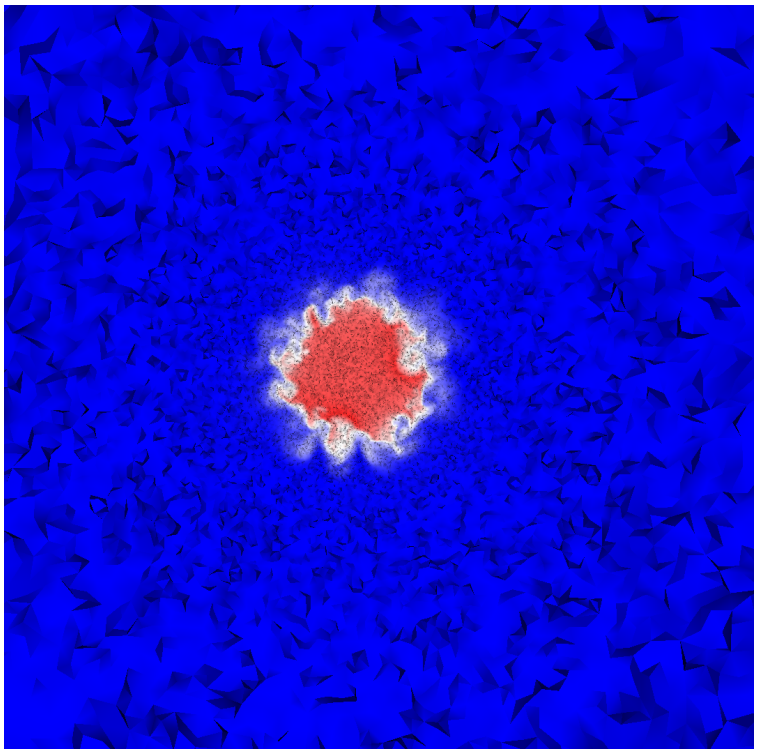

Figure 7. $x = 2D_j$ **slice of the PW1 mesh, colored by instantaneous axial velocity.**

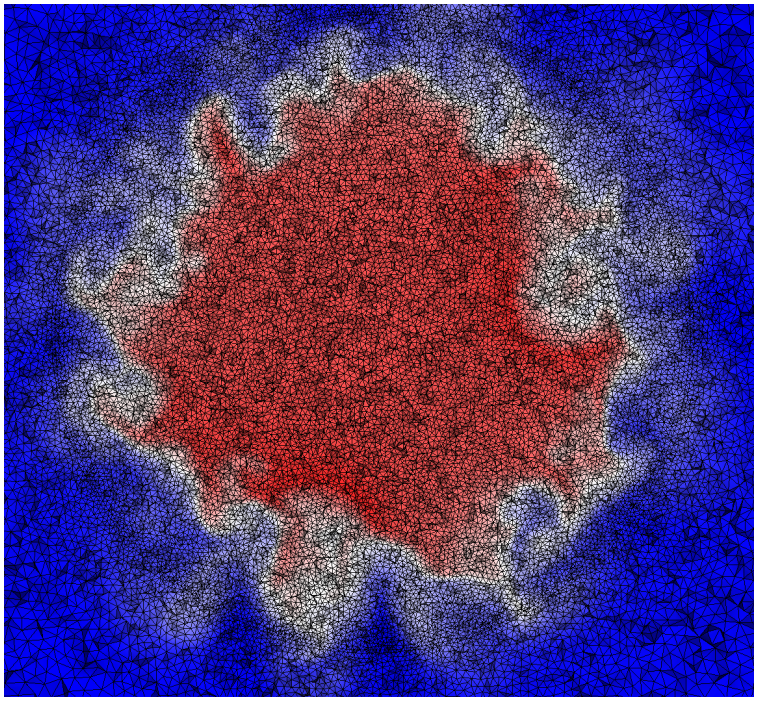

Figure 8. $x = 2D_j$ **slice of the PW1 mesh, colored by instantaneous axial velocity, enlarged figure.**

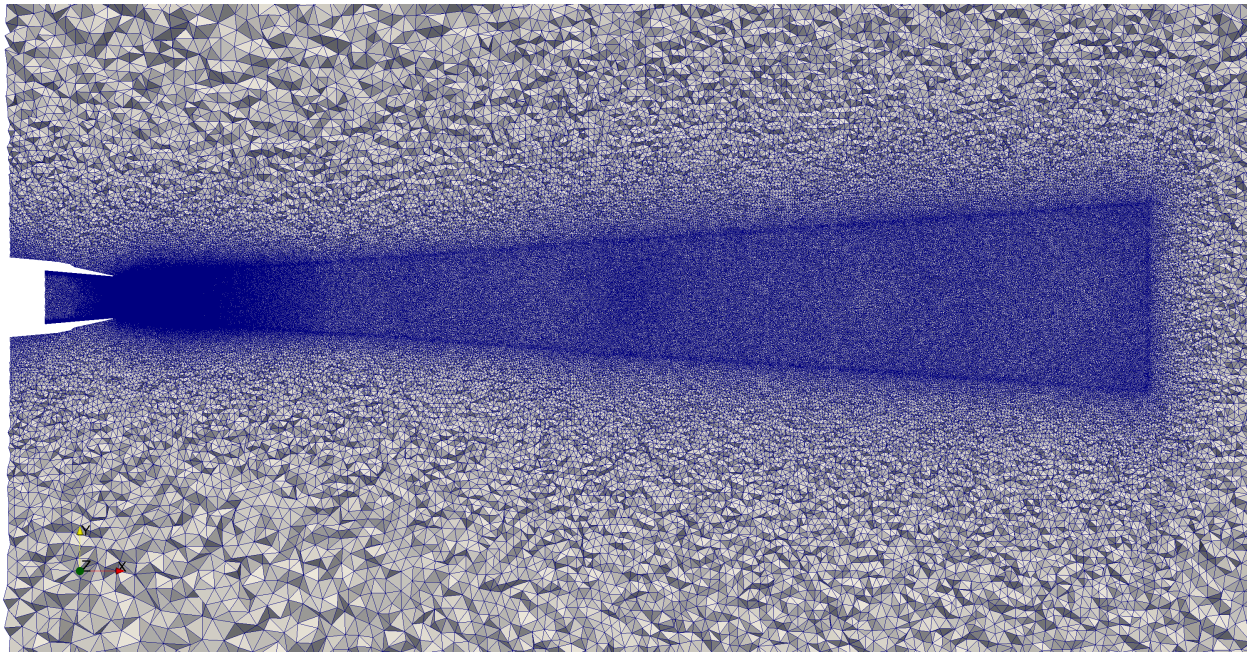

Figure 9. Enlargement of the nearfield region of the $z = 0$ **mesh slice shown in Figure 2 for the PW0 mesh, with cell edges highlighted to make the mesh spacing distribution more clear.**

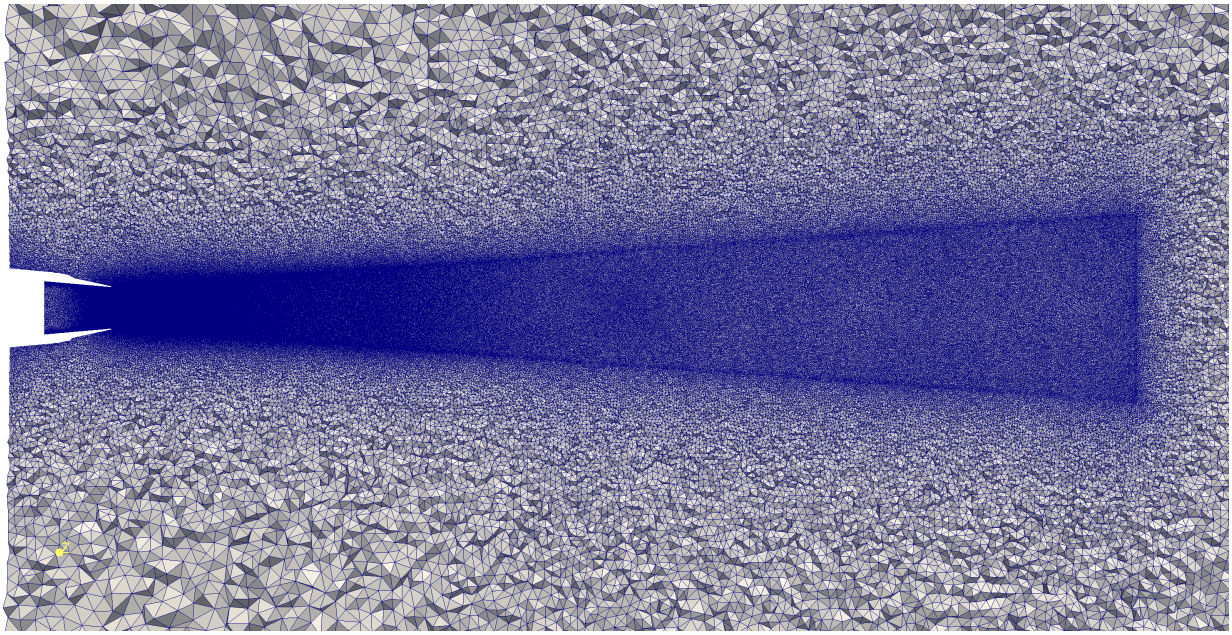

Figure 10. Enlargement of the nearfield region of the $z = 0$ mesh slice shown in Figure 3 for the PW1 mesh, with cell edges highlighted to make the mesh spacing distribution more clear.

thickness growth rates reported by Bridges & Wernet.[46] Figures 6 and 11 seem to show that this choice was adequately large, as do Figures 7 and 8, $x = 2D_j$ slices of the PW1 mesh. The nearfield length L is comparable to[15,16] or longer than[4,5,7,17,19,20] that used by other researchers, but the width of $25D_j \tan(4°)$ is considerably more narrow than similar simulations[4,5,7,17,19,20] found in the literature ($4D_j$ to $7.5D_j$ is typical).

For all meshes, anisotropic tetrahedra were extruded off the interior nozzle walls to partially resolve the boundary layer, likely to be quasi-turbulent according to Bridges and Wernet.[46] For PW0 and PW1, this was done using Pointwise's T-Rex tool, while Gmsh's transfinite interpolation was used for GM0. The spacing of these cells in the wall-normal direction is initially $5 \cdot 10^{-4} D_j$, and grows at a rate of 1.2 until the tetrahedra become isotropic. The length scale of the viscous sublayer for the flows studied here is approximately $y_\tau = 4.1 \cdot 10^{-5} \cdot D_j$ (estimated from smooth flat plate boundary layer theory as described by Schlichting[49]), and thus the simulations will not meet the "wall-resolved" requirement of $\Delta \approx 2y_\tau$.[50]

The minimum mesh spacing in the nozzle nearfield region is $0.01D_j$ for the PW0 mesh, and $0.005D_j$ for the PW1 and GM0. Other subsonic jet LES examples in the literature use minimum mesh spacings ranging from about $0.002{D_j}$[5,20] to $0.003D_j$,[15,16] and past supersonic jet calculations done by NRL researchers used spacings as small as $0.0035D_j$ in shear layer.[29,31] The mesh spacing increases gradually downstream to $0.04D_j$ at the end of the nearfield region for both meshes.

Boundary conditions consisted of adiabatic no-slip for all nozzle walls, and the appropriate constant stagnation pressure and temperature for the set point under investigation for the nozzle inflow. JENRE's characteristic-based farfield boundary condition was used for all other boundaries. As indicated in Figure 1, a sponge zone was used to damp any spurious reflections from these farfield.

III. Results

A. Set point 3

For set point 3 and the two Pointwise meshes, a constant time step was chosen such that the local CFL number would not exceed 0.65 anywhere during the calculation. This time step size was reevaluated periodically during the run (about every 100 steps). The GM0 runs used a constant timestep of $5.13 \cdot 10^{-5} D_j/U_j$, corresponding to a CFL of about 0.24. Each set point 3 run was started from a uniform flow of zero velocity and ambient pressure and temperature. Table 2 shows the amount of time the simulation was run before

	$T_0 \cdot U_j/D_j$	$T \cdot U_j/D_j$
PW0	215.0	300.0
PW1	747.0	547.0
GM0	202.0	145.0

Table 2. Set point 3 startup (T_0) and statistics (T) times.

gathering statistics (T_0) and during the statistics-gathering process (T). The values for $T \cdot U_j/D_j$ for the PW0 and PW1 meshes comparable to the periods of $87.5D_j/U_j$,[20] $500D_j/U_j$,[17] and $833D_j/U_j$[19] found in the literature. GM0, the largest and thus most computationally expensive mesh, may benefit from more time.

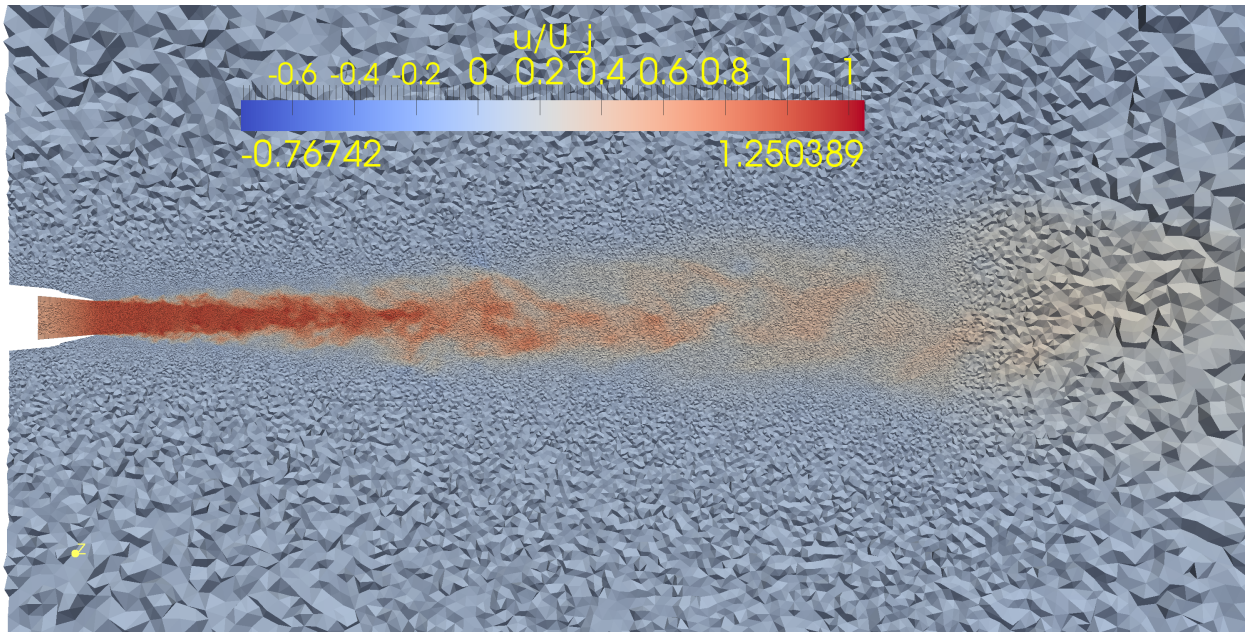

Figure 11. Instantaneous axial velocity non-dimensionalized by U_j for set point 3 run on the PW1 mesh.

After performing the simulations with the JENRE code as described in the previous section, the resulting data was post-processed to obtain mean and RMS statistics of axial velocity, and then compared to Bridges and Wernet's measurements.[46] Figure 11 shows the instantaneous axial velocity from an arbitrary time step for set point 3 on the PW1 mesh, and seems to indicate that the width of the mesh's nearfield region is large enough to capture the majority of the turbulent flow field.

Figure 12 and 13 show the mean and RMS of axial velocity along the centerline of the jet as a function of the distance from the nozzle exit, and compare these values to the "consensus" dataset found in reference,[46] which consists of a representation of an expected value for these quantities informed by experiments run by many researchers performed at multiple labs over a considerable length of time, including to a significant degree by Bridges and Wernet themselves.

Figure 12 shows that little difference is observed between the results for the mean axial velocity $\overline{U}$ along the centerline for the three meshes. All simulations predict the length of the potential core (the region downstream of the nozzle exit that is unaffected by the shear layer) accurately, and consistently underpredict $\overline{U}$ downstream slightly. More spread between the two simulations is seen in Figure 13's root-mean square axial velocity U' results. Both simulations match the experimental data reasonably well for $x < 10D_j$, and show significant dissipation for the region beyond about $x > 15D_j$. Interestingly, the simulation performed on the coarser PW0 mesh agrees better than the the two finer meshes. GM0's RMS results show a bit more variation over $x > 10D_j$, likely a result of the shorter statistics sampling time for this run.

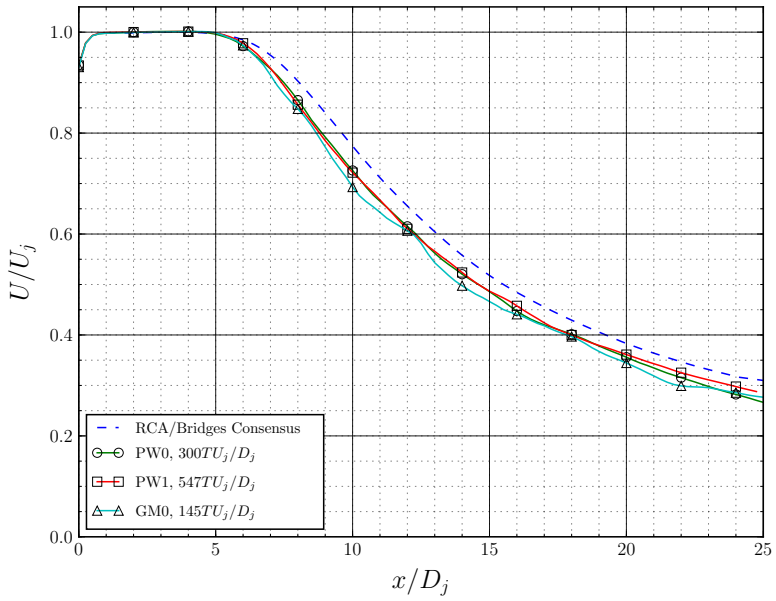

Figure 12. Mean axial velocity $\overline{U}$ along centerline ($r = 0$) for set point 3.

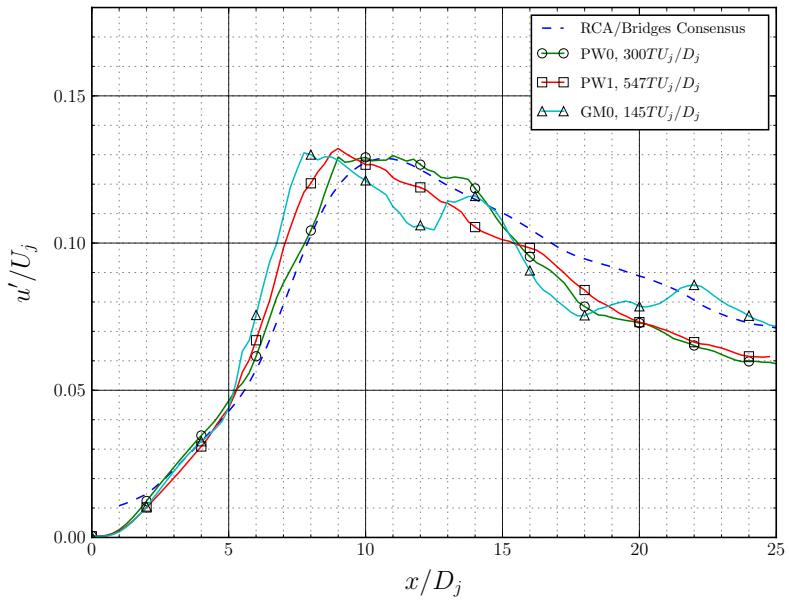

Figure 13. Root-mean square of axial velocity U' along centerline ($r = 0$) for set point 3.

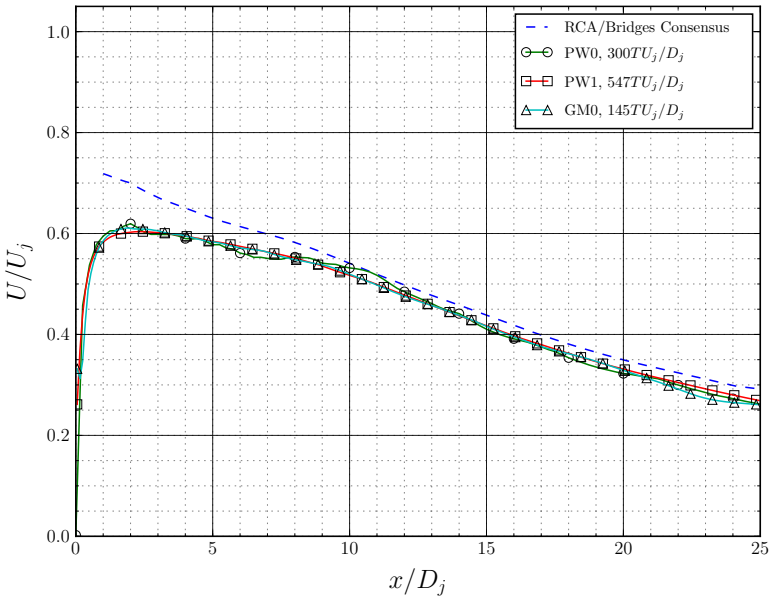

Figure 14. $\overline{U}$ along lipline ($r = D_j/2$) for set point 3.

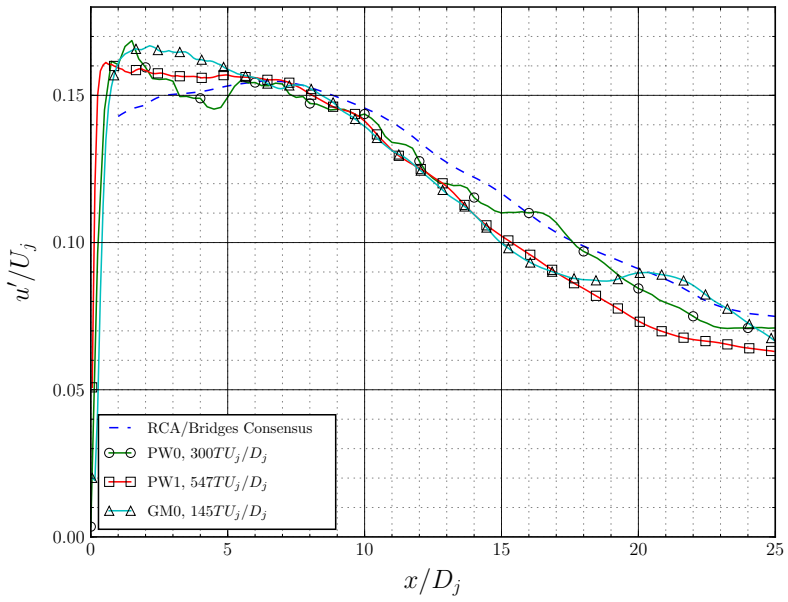

Figure 15. U' along lipline ($r = D_j/2$) for set point 3.

The $\overline{U}$ and U' data along the lipline (i.e., $r = 0.5D_j$) as a function of axial distance from the nozzle are shown in Figures 14 and 15, respectively. Like the $\overline{U}$ centerline results in Figure 12, there is little difference between the three simulations, and all simulations tend to underpredict Bridges & Wernet's measurements, with the largest discrepancy just downstream of the nozzle exit. Figure 15 shows the simulations also have trouble in the same region for the U' data, where a noticeable overshoot in the JENRE predictions is observed. This spike in U' is often observed when the boundary layer unsteadiness in the simulations is too low, leading to the periodic shedding of a large, laminar-like vortex. The magnitude of the spike observed here is smaller than that of other simulations, however.

B. Set point 7

The set point 7 runs, like those of set point 3, were started from uniform flow of zero velocity and ambient pressure and temperature, with the exception of the run on the GM0 mesh, which was started from the end of the corresponding set point 3 run in an attempt to decrease the amount of time needed to reach a statically steady state.. Table 2 shows the amount of time the simulation was run before gathering statistics (T_0) and during the statistics-gathering process (T). With the interest of decreasing the turnaround time of the simulations, the T_0 values are lower than those used for the set point 3 runs.

	$T_0 \cdot U_j/D_j$	$T \cdot U_j/D_j$
PW0	69	170
PW1	67	182
GM0	45*	63

Table 3. Set point 7 startup (T_0) and statistics (T) times. The GM0 run was started from the set point 3 flow at $166D_j/U_j$.

Like the set point 3 simulations, the PW0 and PW1 runs used a constant time step that prevented the CFL number from exceeding 0.5 for the startup period. This approach was also used for the GM0 run, but a lower CFL limit of 0.25 was required to maintain stability. For the statistics-gathering period T, a constant time step was used for all simulations: $1.23 \cdot 10^{-4} D_j/U_j$ for PW0, $1.29 \cdot 10^{-4} D_j/U_j$ for PW1, and $6.95 \cdot 10^{-5} D_j/U_j$ for GM0.

Figures 16 and 17 show the axial velocity mean and RMS results, respectively, for the centerline. The results are very similar to the corresponding set point 3 plots. The potential core is well predicted by all three simulations, and the mean flow after the potential core is slightly under-predicted, with satisfactory agreement overall. The location of the peak RMS is a bit upstream of the experimental data, but not as much as the set point 3 results.

Figures 18 and 19 show the axial velocity mean and RMS results, respectively, for the $r = 0.5D_j$ lipline. Like the centerline results, the data is very similar to set point 3. The mean axial velocity is underpredicted just downstream of the nozzle, but corresponds well to the experimental data otherwise. There is a small RMS spike just downstream of the nozzle exit, and the RMS data is lower than the experiment for $x > 12D_j$, and may benefit from more simulation time, especially the GM0 mesh.

C. Set point 23

The preliminary set point 23 run was initiated from the last time step of the set point 3 calculation, with the goal of reducing the amount of time needed for the flow to reach a statistically stationary state. This set point has only been performed on the PW1 mesh to date (the finest mesh available at the time the simulations were started). The JENRE data was post-processed for the same $\overline{U}$ and U' statistics presented in the setpoint 3 section, and also for the mean and RMS temperature data ($\overline{T}$ and T', respectively) along the nozzle centerline and lipline. The temperature statistics were compared to Rayleigh scattering measurements performed by Mielke & Elam.[51]

Figures 20 and 21 show $\overline{U}$ and U' for the setpoint 23 case, respectively. The agreement between the JENRE and experimental data is striking in the $\overline{U}$ plot. The U' results in Figure 21 do not show the same excellent correspondence with the measurements, but still agree fairly satisfactorily with the experimental data. Interestingly, for the $x > 10D_j$ region, JENRE's U' prediction is *better* than what is observed for

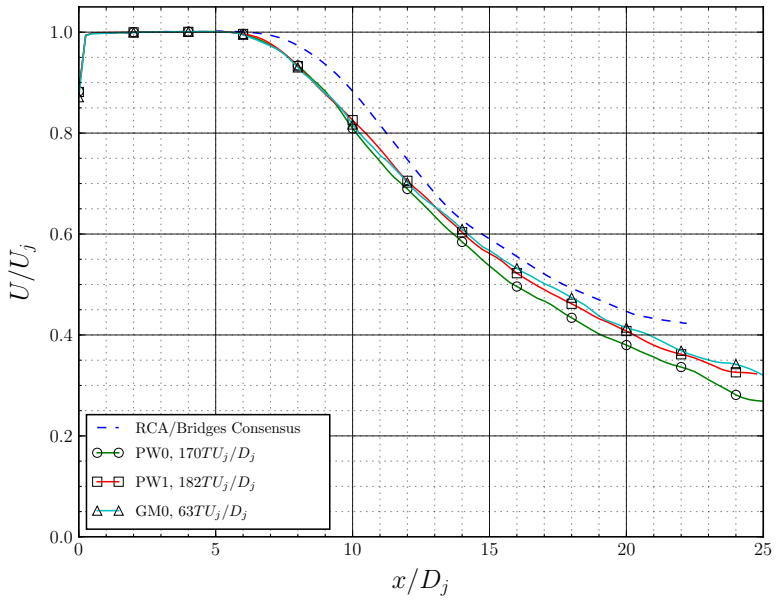

Figure 16. Mean axial velocity $\overline{U}$ along centerline ($r = 0$) for set point 7.

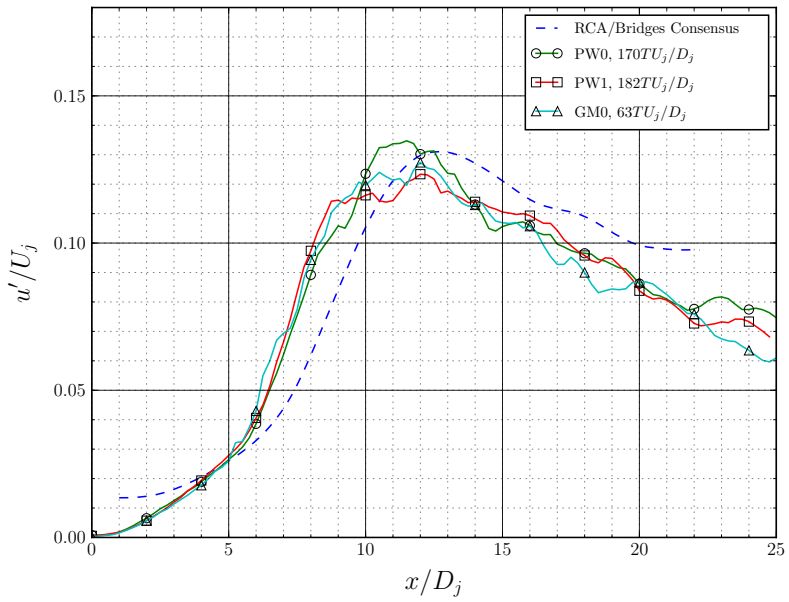

Figure 17. Root-mean square of axial velocity U' along centerline ($r = 0$) for set point 7.

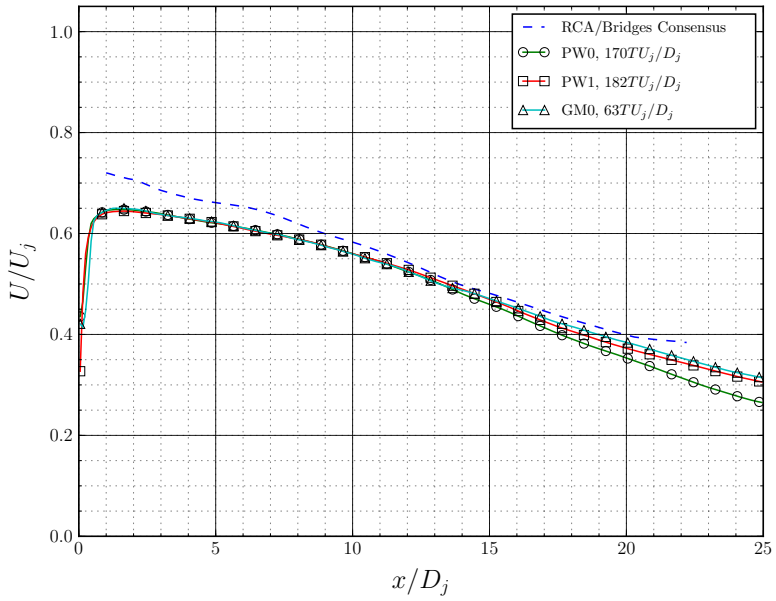

Figure 18. $\overline{U}$ along lipline ($r = D_j/2$) for set point 7.

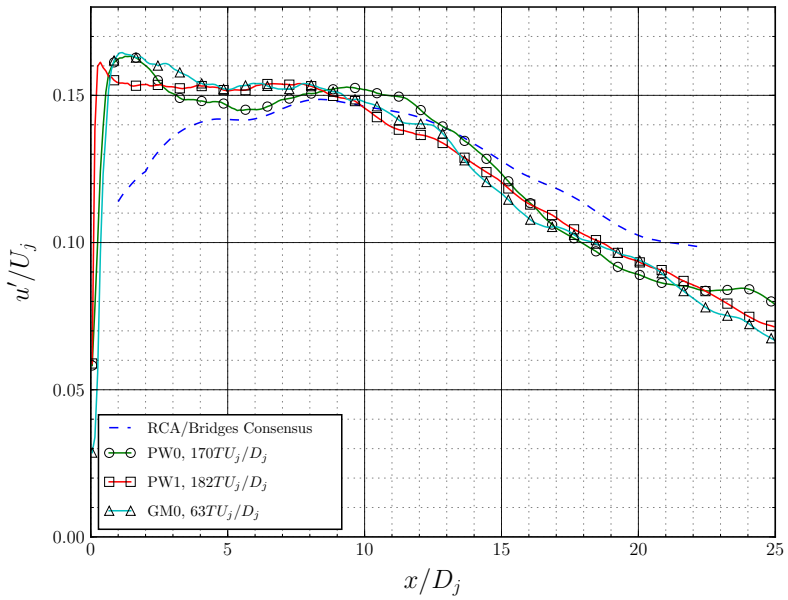

Figure 19. U' along lipline ($r = D_j/2$) for set point 7.

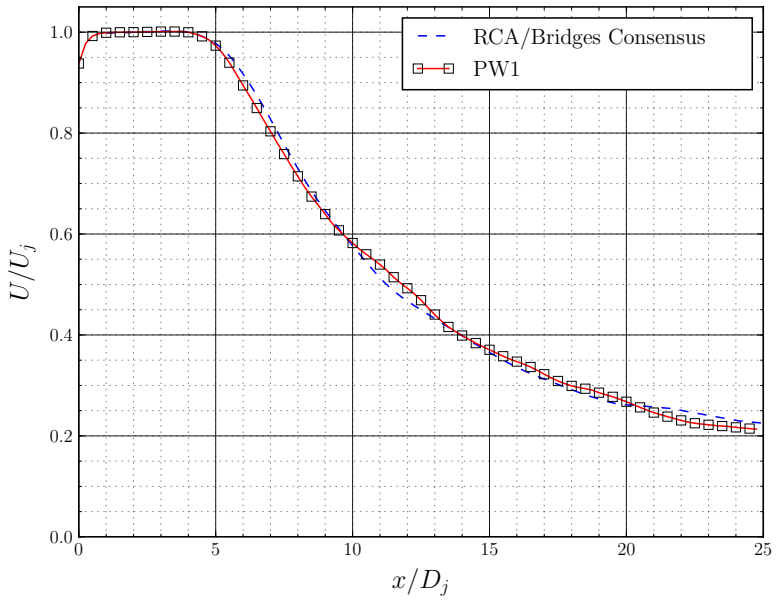

Figure 20. $\overline{U}$ along centerline ($r = 0$) for setpoint 23.

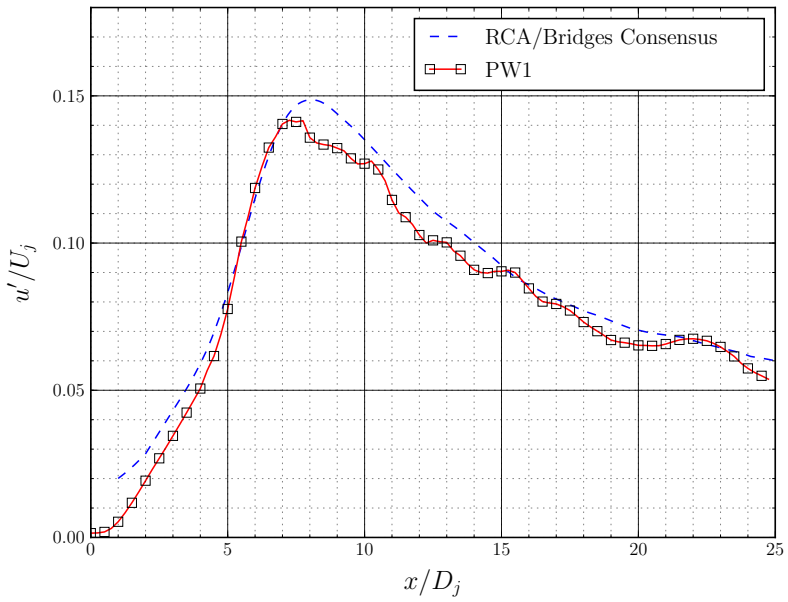

Figure 21. U' along centerline ($r = 0$) for setpoint 23.

setpoint 3 in Figure 13. Comparison between the U' experimental data for the two set points seems to show that the heated jet case tends to have lower axial velocity fluctuations in the $x > 10D_j$ region, perhaps due to the more intense mixing associated with the hot jet's temperature gradients.

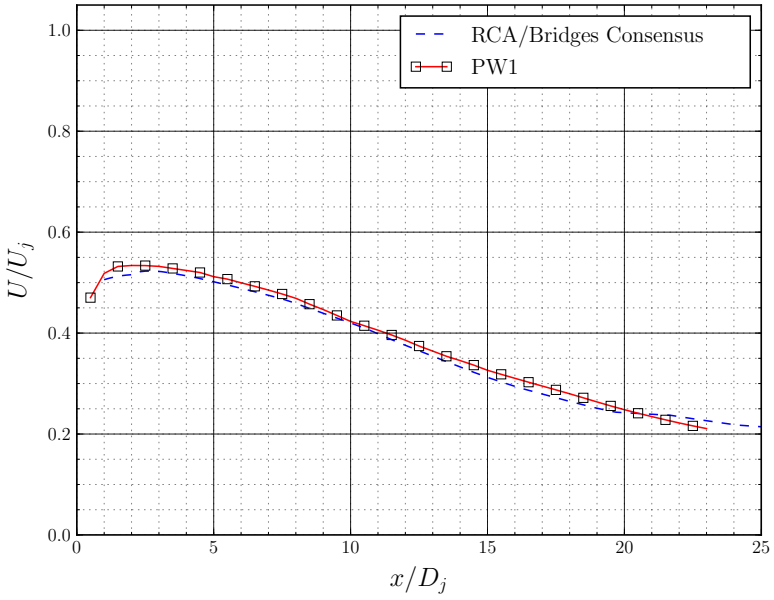

Figure 22. $\overline{U}$ along lipline ($r = D_j/2$) for setpoint 23.

The $\overline{U}$ and U' lipline data for the setpoint 23 simulation are shown in Figures 22 and 23, respectively. Again, JENRE's prediction for $\overline{U}$ closely approximates Bridges and Wernet's measurements, and the U' agreement is also fairly good. Interestingly, the overshoot just downstream of the nozzle exit seen in setpoint 3's U' lipline data (Figure 15) is not observed for this flow condition.

Figures 20 and 25 contain mean and RMS temperature data ($\overline{T}$ and T', respectively) along the centerline, along with the Rayleigh scattering measurements from Mielke and Elam.[51] The $\overline{T}$ data agrees well for $x \leq 7D_j$, but diverges from the measured values for $x > 7D_j$, where it is a bit higher than the experiment. Similarly, the T' data in Figure 25 agrees well for $x < 10D_j$, but not for the points further downstream. (Mielke cautions[52] that the data downstream of $x = 10D_j$ my be contaminated by particles from the ambient flow, which would interfere with the Rayleigh scattering technique used for the temperature measurement.)

The $\overline{T}$ and T' statistics for the lipline region for the present setpoint are shown in Figures 26 and 27, respectively. JENRE's $\overline{T}$ data follows the experimental trend fairly well, but is shifted up for the entire axial range. Finally, the T' data is somewhat close to Mielke & Elam's measurements in the region just downstream of the nozzle exit, but does not compare well as x increases. Again, Mielke[52] indicates a higher uncertainty for the data in this region. More investigation is needed.

IV. Conclusions and Future Work

This paper has presented the preliminary results of applying the JENRE code to the task of predicting the nearfield turbulence of three subsonic jets. Three meshes of the SMC000 geometry were generated and then used with the JENRE LES code to simulate set points 3 and 7 from the Tanna test matrix, with one mesh also used to simulate set point 23. Good agreement between the JENRE data and experimental measurements was observed for the axial velocity statistics in the nearfield, indicating that JENRE holds promise as a LES/CAA tool. JENRE's results for the mean axial velocity along both the lipline and centerline closely followed the experimental data for all three set points. The RMS axial velocity agreement was also quite good, but may benefit from a bit more simulation time. Interestingly, little difference between the results for PW0 (the coarsest mesh, with a minimum shear layer mesh spacing of $0.01D_j$) and PW1 and

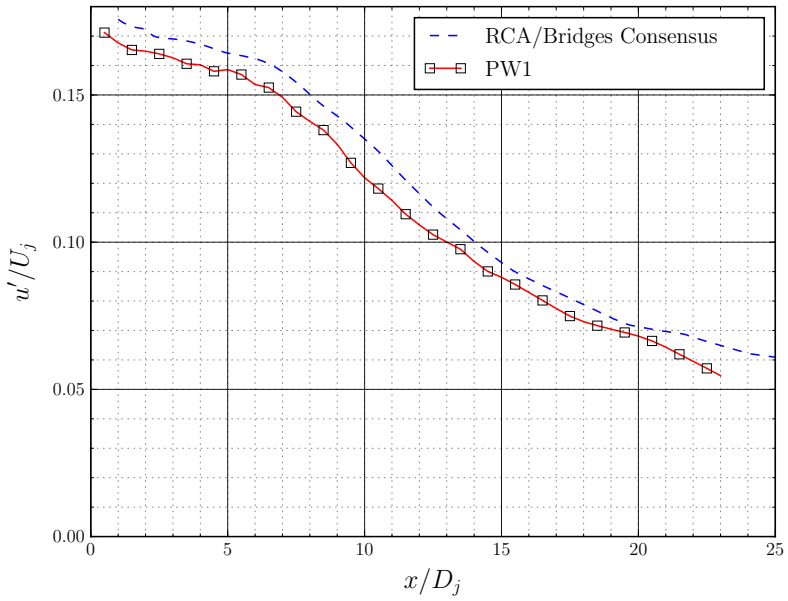

Figure 23. U' along lipline ($r = D_j/2$) for setpoint 23.

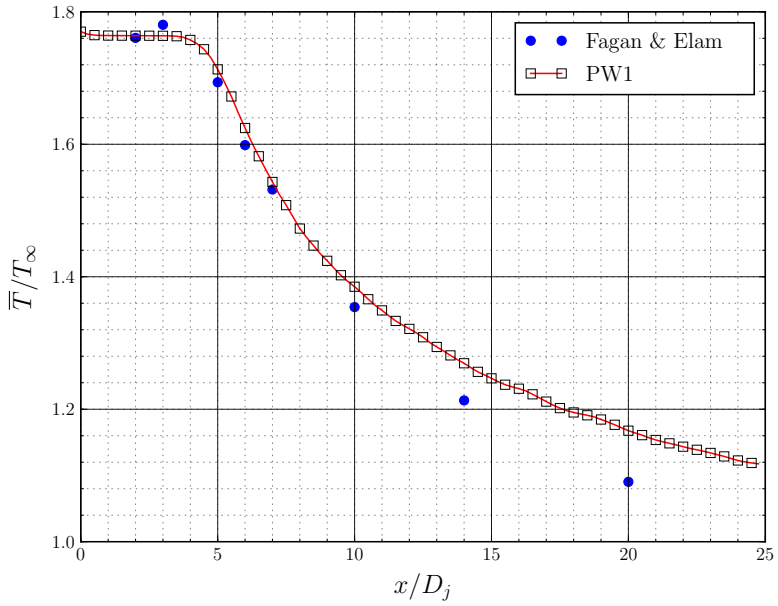

Figure 24. Mean temperature $\overline{T}$ along centerline ($r = 0$) for setpoint 23.

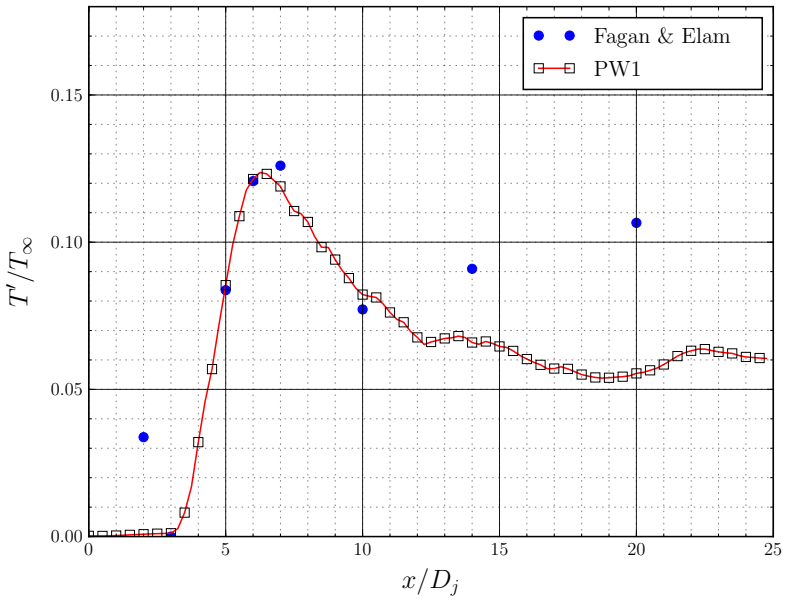

Figure 25. RMS of temperature T' along centerline ($r = 0$) for setpoint 23.

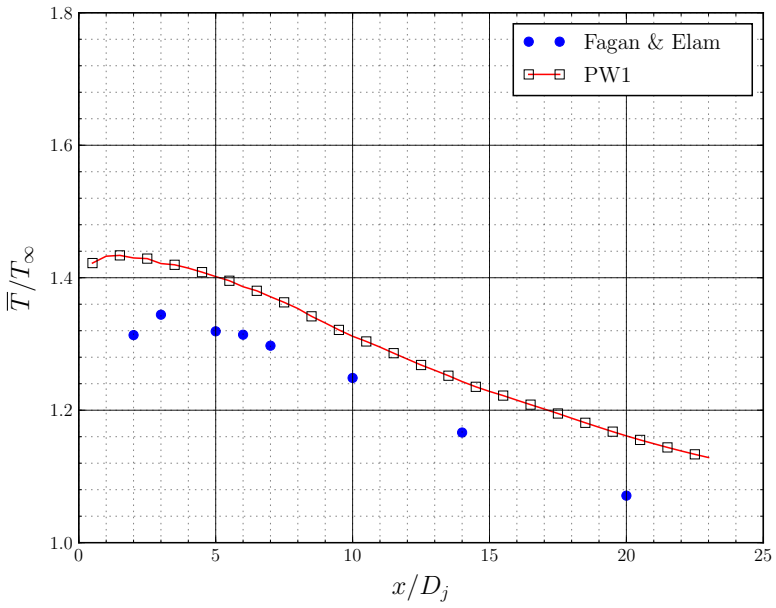

Figure 26. $\overline{T}$ along lipline ($r = D_j/2$) for setpoint 23.

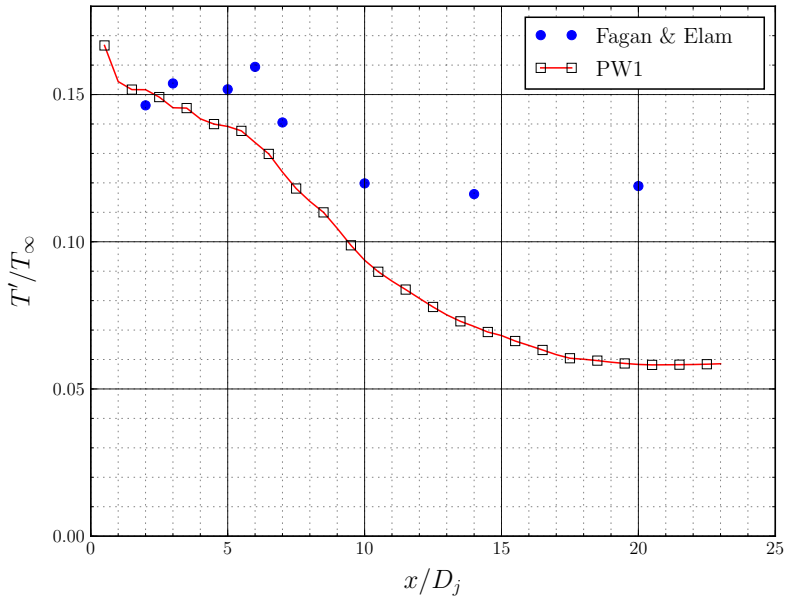

Figure 27. T' **along lipline** ($r = D_j/2$) **for setpoint 23.**

GM0 (minimum shear layer spacing of $0.005D_j$) was observed for the turbulent statistics presented here — though it remains to be seen if this is true for the planned acoustic predictions.

In the future, JENRE's Ffowcs-Williams Hawking (FW-H) solver will be used to obtain farfield acoustic predictions. Figure 28 shows the proposed location of the FW-H integration surface superimposed on the non-dimensional vorticity magnitude for the PW0 mesh. Following the advice of Erwin and Sinha,[53] the surface has been placed where the vorticity falls below 0.5, which should hopefully keep the integration surface outside of the region where hydrodynamic pressure fluctuations are present. For this first attempt at farfield noise predictions, no endcaps or disk averaging will be used at the FW-H surface outflow — it is hoped that the surface will be long enough to contain all the significant jet noise sources.

Acknowledgements

This work has been supported by the NASA Commercial Supersonics Technology Project, part of the Advanced Air Vehicles Program. Help from NRL researchers Andrew Corrigan, Junhui Liu, Kamal Viswanath, Ravi Ramamurti, Ryan Johnson, and Kailas Kailasanath was essential in preparing the JENRE simulations described in this work. Resources supporting this work were provided by the NASA High-End Computing (HEC) Program through the NASA Advanced Supercomputing (NAS) Division at Ames Research Center.

References

[1]Andersson, N., Eriksson, L.-E., and Davidson, L., "Investigation of an isothermal Mach 0.75 jet and its radiated sound using large-eddy simulation and Kirchhoff surface integration," *International Journal of Heat and Fluid Flow*, Vol. 26, No. 3, jun 2005, pp. 393–410.

[2]Apte, S. V., Mahesh, K., Moin, P., and Oefelein, J. C., "Large-eddy simulation of swirling particle-laden flows in a coaxial-jet combustor," *International Journal of Multiphase Flow*, Vol. 29, No. 8, aug 2003, pp. 1311–1331.

[3]Bodony, D. J. and Lele, S. K., "On using large-eddy simulation for the prediction of noise from cold and heated turbulent jets," *Physics of Fluids (1994-present)*, Vol. 17, No. 8, aug 2005, pp. 085103.

[4]Bogey, C. and Bailly, C., "Effects of Inflow Conditions and Forcing on Subsonic Jet Flows and Noise." *AIAA Journal*, Vol. 43, No. 5, 2005, pp. 1000–1007.

[5]Bogey, C., Marsden, O., and Bailly, C., "Effects of initial shear-layer thickness on turbulent subsonic jets at moderate Reynolds numbers," American Institute of Aeronautics and Astronautics, jun 2012.

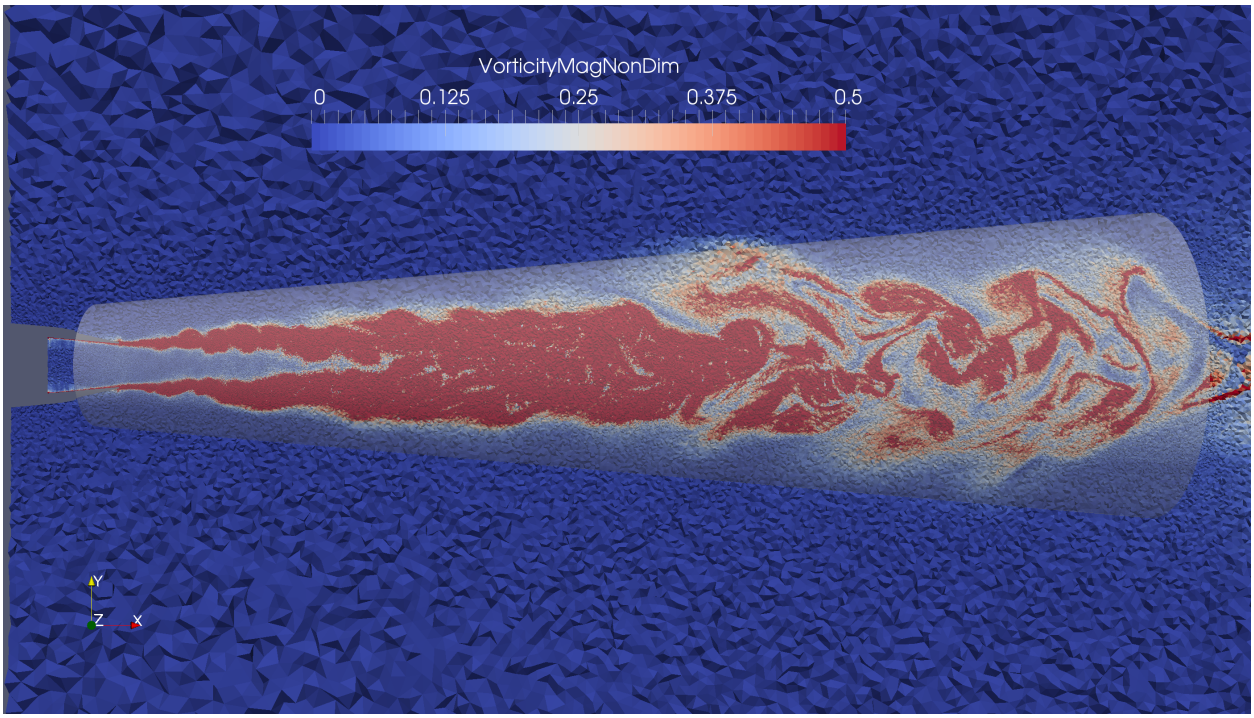

Figure 28. $z = 0$ slice of the PW0 mesh, colored by non-dimensional vorticity magnitude, superimposed with the proposed FW-H surface.

[6]Bogey, C. and Bailly, C., "Investigation of Subsonic Jet Noise Using LES: Mach and Reynolds Number Effects," American Institute of Aeronautics and Astronautics, may 2004.

[7]Bogey, C. and Bailly, C., "Investigation of downstream and sideline subsonic jet noise using Large Eddy Simulation," *Theoretical and Computational Fluid Dynamics*, Vol. 20, No. 1, feb 2006, pp. 23–40.

[8]Bogey, C. and Bailly, C., "Large eddy simulations of transitional round jets: influence of the Reynolds number on flow development and energy dissipation," *Physics of Fluids (1994-present)*, Vol. 18, No. 6, 2006, pp. 065101.

[9]Bogey, C. and Bailly, C., "LES of a High Reynolds, High Subsonic Jet: Effects of the Subgrid Modellings on Flow and Noise," American Institute of Aeronautics and Astronautics, jun 2003.

[10]Bogey, C. and Bailly, C., "LES of a High Reynolds, High Subsonic Jet: Effects of the Inflow Conditions on Flow and Noise," American Institute of Aeronautics and Astronautics, may 2003.

[11]Bogey, C., Bailly, C., and Juvé, D., "Noise Investigation of a High Subsonic, Moderate Reynolds Number Jet Using a Compressible Large Eddy Simulation," *Theoretical and Computational Fluid Dynamics*, Vol. 16, No. 4, mar 2003, pp. 273–297.

[12]Freund, J. B., "Noise sources in a low-Reynolds-number turbulent jet at Mach 0.9," *Journal of Fluid Mechanics*, Vol. 438, jul 2001, pp. 277–305.

[13]Li, Q., Page, G., and McGuirk, J., "LES of Impinging Jet Flows Relevant to Vertical Landing Aircraft Using an Unstructured Mesh Approach," American Institute of Aeronautics and Astronautics, jun 2006.

[14]Lyrintzis, A. S. and Blaisdell, G. A., "Jet Noise Predictions Using Large Eddy Simulations," *2nd International Conference on Fluid Mechanics and Heat & Mass Transfer*, 2011, pp. 14–16.

[15]Shur, M., Spalart, P., and Strelets, M., "Noise prediction for increasingly complex jets. Part II: Applications," *International Journal of Aeroacoustics*, Vol. 4, No. 3, 2005, pp. 247–266.

[16]Shur, M., Spalart, P., and Strelets, M., "Noise prediction for increasingly complex jets. Part I: Methods and tests," *International Journal of Aeroacoustics*, Vol. 4, No. 3, 2005, pp. 213–246.

[17]Uzun, A., Lyrintzis, A., and Blaisdell, G., "Coupling of Integral Acoustics Methods With LES for Jet Noise Prediction," *International Journal of Aeroacoustics*, Vol. 3, No. 4, oct 2004, pp. 297–346.

[18]Zhao, W., Frankel, S. H., and Mongeau, L., "Large Eddy Simulations of Sound Radiation from Subsonic Turbulent Jets," *AIAA Journal*, Vol. 39, No. 8, 2001, pp. 1469–1477.

[19]Bogey, C. and Bailly, C., "Computation of a high Reynolds number jet and its radiated noise using large eddy simulation based on explicit filtering," *Computers & Fluids*, Vol. 35, No. 10, 2006, pp. 1344 – 1358.

[20]Bogey, C., Marsden, O., and Bailly, C., "Large-eddy simulation of the flow and acoustic fields of a Reynolds number 10[sup 5] subsonic jet with tripped exit boundary layers," *Physics of Fluids*, Vol. 23, No. 3, 2011, pp. 035104.

[21]Bodony, D. J. and Lele, S. K., "Current Status of Jet Noise Predictions Using Large-Eddy Simulation," *AIAA Journal*, Vol. 46, No. 2, 2008, pp. 364–380.

[22]Khalighi, Y., Ham, F., Nichols, J., Lele, S., and Moin, P., "Unstructured Large Eddy Simulation for Prediction of Noise Issued from Turbulent Jets in Various Configurations," *17th AIAA/CEAS Aeroacoustics Conference (32nd AIAA Aeroacoustics Conference)*, American Institute of Aeronautics and Astronautics (AIAA), Jun 2011.

[23]Nichols, J., Lele, S., Moin, P., Ham, F., Brès, G., and Bridges, J., "Large-eddy simulation for supersonic rectangular jet noise prediction: effects of chevrons," *18th AIAA/CEAS Aeroacoustics Conference (33rd AIAA Aeroacoustics Conference)*, American Institute of Aeronautics and Astronautics (AIAA), Jun 2012.

[24]Brès, G., Nichols, J., Lele, S., Ham, F., Schlinker, R., Reba, R., and Simonich, J., "Unstructured Large Eddy Simulation of a Hot Supersonic Over-Expanded Jet with Chevrons," *18th AIAA/CEAS Aeroacoustics Conference (33rd AIAA Aeroacoustics Conference)*, American Institute of Aeronautics and Astronautics (AIAA), Jun 2012.

[25]Brès, G., Nichols, J., Lele, S., and Ham, F., "Towards Best Practices for Jet Noise Predictions with Unstructured Large Eddy Simulations," *42nd AIAA Fluid Dynamics Conference and Exhibit*, American Institute of Aeronautics and Astronautics (AIAA), Jun 2012.

[26]Brès, G. A., Ham, F., Nichols, J. W., and Lele, S. K., "Nozzle Wall Modeling in Unstructured Large Eddy Simulations for Hot Supersonic Jet Predictions," *19th AIAA/CEAS Aeroacoustics Conference*, American Institute of Aeronautics and Astronautics (AIAA), May 2013.

[27]Liu, J., Kailasanath, K., Ramamurti, R., Munday, D., Gutmark, E., and Lohner, R., "Large-Eddy Simulations of a Supersonic Jet and Its Near-Field Acoustic Properties," *AIAA Journal*, Vol. 47, No. 8, 2009, pp. 1849–1865.

[28]Liu, J., Kailasanath, K., Boris, J., Heeb, N., Munday, D., and Gutmark, E., "Effect of Nozzle-exit Flow Conditions on the Flow and Acoustic Properties of Imperfectly Expanded Supersonic Jets," *18th AIAA/CEAS Aeroacoustics Conference (33rd AIAA Aeroacoustics Conference)*, American Institute of Aeronautics and Astronautics (AIAA), Jun 2012.

[29]Liu, J., Corrigan, A. T., Kailasanath, K., Heeb, N. S., Munday, D. E., and Gutmark, E. J., "Computational Study of Shock-Associated Noise Characteristics Using LES," American Institute of Aeronautics and Astronautics, may 2013.

[30]Junhui Liu, Andrew T. Corrigan, Kailas Kailasanath, Nicholas S. Heeb, and Ephraim J. Gutmark, "Numerical Study of Noise Sources Characteristics in An Underexpanded Jet Flow," *20th AIAA/CEAS Aeroacoustics Conference*, AIAA Aviation, American Institute of Aeronautics and Astronautics, jun 2014.

[31]Liu, J., Corrigan, A. T., Kailasanath, K., Heeb, N. S., Munday, D. E., and Gutmark, E. J., "Computational Study of the Impact of Chevrons on Noise Characteristics of Imperfectly Expanded Jet Flows," American Institute of Aeronautics and Astronautics, jan 2014.

[32]Ramamurti, R., Corrigan, A. T., Liu, J., Kailasanath, K., and Henderson, B. S., "Computational Study of the Effect of Slotted Air Injection on Jet Noise," *20th AIAA/CEAS Aeroacoustics Conference*, American Institute of Aeronautics and Astronautics (AIAA), jun 2014.

[33]Junhui Liu, Andrew T. Corrigan, Kailas Kailasanath, and Ephraim J. Gutmark, "Impact of Chevrons on Noise Source Characteristics In Imperfectly Expanded Jet Flows," *21st AIAA/CEAS Aeroacoustics Conference*, AIAA Aviation, American Institute of Aeronautics and Astronautics, jun 2015.

[34]Lyrintzis, A., "Surface integral methods in computational aeroacoustics—From the (CFD) near-field to the (Acoustic) far-field," *International Journal of Aeroacoustics*, Vol. 2, No. 2, 2003, pp. 95–128.

[35]Leib, S. J., Ingraham, D., and Bridges, J., "Evaluating Source Terms of the Generalized Acoustic Analogy using the Jet Engine Noise REduction (JENRE) Code," *55th AIAA Aerospace Sciences Meeting*, American Institute of Aeronautics and Astronautics (AIAA), Jan 2017 (submitted).

[36]Kailas Kailasanath, Andrew T. Corrigan, Junhui Liu, and Ravi Ramamurti, "Efficient Supersonic Jet Noise Simulations Using JENRE," *50th AIAA/ASME/SAE/ASEE Joint Propulsion Conference*, Propulsion and Energy Forum, American Institute of Aeronautics and Astronautics, jul 2014.

[37]Grinstein, F. F. and Fureby, C., "On Monotonically Integrated Large Eddy Simulation of Turbulent Flows Based on FCT Algorithms," *Flux-Corrected Transport*, Springer Science + Business Media, 2005, pp. 79–104.

[38]Fernando F. Grinstein, Len G. Margolin, and William J. Rider, *Implicit Large Eddy Simulation: Computing Turbulent Fluid Dynamics*, chap. A Rationale for Implicit LES, Cambridge University Press, 2007, pp. 39–58.

[39]Oran, E. S. and Boris, J. P., "Computing Turbulent Shear Flows — A Convenient Conspiracy," *Computers in Physics*, Vol. 7, No. 5, 1993, pp. 523–533.

[40]Boris, J. P., *Implicit Large Eddy Simulation: Computing Turbulent Fluid Dynamics*, chap. More for LES: A Brief Historical Perspective of MILES, Cambridge University Press, 2007, pp. 9–38.

[41]Donea, J., "A Taylor-Galerkin method for convective transport problems," *International Journal for Numerical Methods in Engineering*, Vol. 20, No. 1, jan 1984, pp. 101–119.

[42]Löhner, R., Morgan, K., and Zienkiewicz, O., "An adaptive finite element procedure for compressible high speed flows," *Computer Methods in Applied Mechanics and Engineering*, Vol. 51, No. 1, 1985, pp. 441 – 465.

[43]Löhner, R., Morgan, K., Vahdati, M., Boris, J. P., and Book, D. L., "FEM-FCT: Combining unstructured grids with high resolution," *Communications in Applied Numerical Methods*, Vol. 4, No. 6, nov 1988, pp. 717–729.

[44]Tanna, H., "An experimental study of jet noise part I: Turbulent mixing noise," *Journal of Sound and Vibration*, Vol. 50, No. 3, feb 1977, pp. 405–428.

[45]Brown, C. and Bridges, J., "Small Hot Jet Acoustic Rig Validation," Tech. Rep. NASA/TM-2006-214234, NASA Glenn Research Center, Cleveland, OH, United States, April 2006.

[46]Bridges, J. and Wernet, M. P., "The NASA Subsonic Jet Particle Image Velocimetry (PIV) Dataset," Tech. Rep. NASA/TM 2011-216807, NASA Glenn Research Center, Cleveland, OH, United States, nov 2011.

[47]Pointwise, I., "Pointwise Mesh Generator," `http://www.pointwise.com/`, 2016, Accessed 2016-05-20.

[48]Geuzaine, C. and Remacle, J.-F., "Gmsh: A 3-D finite element mesh generator with built-in pre- and post-processing facilities," *International Journal for Numerical Methods in Engineering*, Vol. 79, No. 11, 2009, pp. 1309–1331.

[49]Schlichting, H. T., *Boundary Layer Theory*, McGraw-Hill, New York, 7th ed., 1979.

[50]Fureby, C., Alin, N., Wikström, N., Menon, S., Svanstedt, N., and Persson, L., "Large Eddy Simulation of High-Reynolds-Number Wall Bounded Flows," *AIAA Journal*, Vol. 42, No. 3, mar 2004, pp. 457–468.

[51]Mielke, A. F. and Elam, K. A., "Dynamic measurement of temperature, velocity, and density in hot jets using Rayleigh scattering," *Experiments in Fluids*, Vol. 47, No. 4-5, Jul 2009, pp. 673–688.

[52]Fagan, A., personal communication, Jan 2016.

[53]Erwin, J. P. and Sinha, N., "Near and Far-Field Investigations of Supersonic Jet Noise Predictions Using a Coupled LES and FW-H Equation Method," *Proceedings of ASME Turbo Expo 2011*, ASME International, 2011.